Available online at www.sciencedirect.com
SCIENCE DIRECT®
International Journal of Heat and Fluid Flow 24 (2003) 356–371
International Journal of HEAT AND FLUID FLOW
www.elsevier.com/locate/ijhff

Direct numerical simulation of heat transfer over riblets

E. Stalio *, E. Nobile

Dipartimento di Ingegneria Navale, del Mare e per l'Ambiente—Sezione di Fisica Tecnica, Università di Trieste, Via A. Valerio 10, 34127 Trieste, Italy

Received 10 March 2002; accepted 1 February 2003

Abstract

Riblets are well-known as a passive mean for drag reduction in turbulent flow conditions, but their effectiveness for heat transfer is quite controversial. In this paper we present the numerical results for fully developed laminar and turbulent flow and heat transfer in a channel with triangular riblets. The turbulent study is performed by means of direct numerical simulation at a Reynolds number $Re_\tau = 180$ based on the wall-shear velocity, for a fluid with a Prandtl number $Pr = 0.71$. Four different ribbed channels are considered, under a constant heat flux boundary condition, and correspond to ridge angle $\alpha = 45°$ and 60°, and riblet spacing $s^+ = 20$ and $s^+ = 40$. The results obtained, for the flow and turbulent quantities, are in good agreement with past experimental and numerical studies, and correctly reproduce drag reduction over the smaller $s^+ = 20$ riblets and drag increase over the larger $s^+ = 40$ riblets. The predicted heat transfer efficiency of riblets do not agree with some experimental results, and is below that of a flat plate for all the configurations. The conditions for heat transfer enhancement are discussed.

Keywords: Turbulent flow; Heat transfer enhancement; Riblets; DNS

1. Introduction

Riblets are formed by streamwise ridges of different cross-section (i.e. triangular, rectangular, L-shaped, etc.) and when correctly designed and sized (Baron et al., 1989), present the favourable property of reducing the friction drag by as much as 8% in turbulent flow conditions (Walsh, 1982), despite the increase of the wetted surface area. Such drag reduction occurs only in turbulent regime, while a drag increase is invariably obtained in laminar conditions (Choi et al., 1991).

The potential applications of riblets were furthermore confirmed in several practical cases (Coustols, 1998), like a full scale flight test on an Airbus A320, and the turbulent flow in internally grooved pipes, where significant reductions in drag were measured. While several works (Choi et al., 1993) have extended the knowledge about the mechanisms associated with the drag reduction, some questions, like the origin and the net effects of the mean secondary flow, are still matter of debate (Goldstein and Tuan, 1998).

In heat transfer applications it is still unclear whether it is possible to obtain a surface geometry that decreases the skin friction, while augmenting the heat transfer coefficient. The remarkable property of riblets to reduce the drag while increasing the wetted surface area, makes riblet-covered walls a potential candidate for effective heat transfer applications. It is then important to evaluate whether riblets, with different cross-sections, might increase the so called Reynolds analogy factor, defined as $2St/C_f$, where St is the Stanton number and C_f is the skin-friction coefficient, beyond that on a smooth wall.

The effectiveness of riblets for heat transfer was only recently experimentally investigated, however these studies did not clearly establish whether riblets, with different cross-section, produce a net variation in heat transfer in comparison to the flat plate value. The first comprehensive experimental investigation, which considered riblets of different cross-shape and size, was carried out by Walsh and Weinstein (1979); a heat transfer coefficient 10% larger than that of a smooth surface was measured, within the drag reducing regime of the riblets $s^+ \leqslant 30$, where $s^+ = su_\tau/v$ and s is the width of the riblet. Lindemann (1985), who experimentally studied the heat transfer efficiency for various surface geometries, discovered that the triangular riblets

* Corresponding author. Tel.: +39-040-558-3817; fax: +39-040-572-033.
E-mail address: stalio@univ.trieste.it (E. Stalio).

0142-727X/03/$ - see front matter © 2003 Elsevier Science Inc. All rights reserved.
doi:10.1016/S0142-727X(03)00004-3

Nomenclature

A	area
$c(\beta,\gamma)$	correlation coefficient between β and γ
c	specific heat
C_f	skin-friction coefficient
D	drag force on the wall
h	riblet height
L_x, L_y, L_z	length of the domain in x, y, z direction
n	coordinate normal to the wall surface
Nu	Nusselt number, Eq. (8)
N_x, N_y, N_z	number of grid points in x, y, z direction
p	periodic part of the pressure field
p^*	pressure field
Pr	molecular Prandtl number, $Pr = \nu/\kappa$
q_w	wall heat-flux
$Re_{4\delta}$	bulk Reynolds number, $Re_{4\delta} = 4\delta u_m/\nu$
Re_τ	Reynolds number based on friction velocity, $Re_\tau = u_\tau\delta/\nu$
s^+	dimensionless riblet spacing, $s^+ = u_\tau s/\nu$
St	Stanton number, Eq. (9)
T	periodic part of the temperature field
T^*	temperature field
T_τ	friction temperature, $T_\tau = q_w/(\rho c u_\tau)$
t	time
t_{ref}	reference time, $t_{ref} = \delta/u_\tau$
u	streamwise velocity component
$\mathbf{u}$	velocity vector
u_τ	friction velocity, $u_\tau = (\tau_w/\rho)^{1/2}$
v	wall normal velocity component
w	spanwise velocity component
$\mathbf{x}$	unit vector for the streamwise coordinate
x, y, z	Cartesian coordinates
y_w	vertical distance from the solid wall

Greeks

α	ridge angle (deg)
ΔT_f	difference between the flat wall mean temperature and the bulk temperature
ΔT_r	difference between the riblet mean temperature and the bulk temperature
ΔT_{fr}	difference between the two temperature drops $\Delta T_f - \Delta T_r$
Δt	computational time-step
δ	half-channel height
η	efficiency
κ	molecular thermal diffusivity
ν	kinematic viscosity
ρ	density
τ_w	wall shear stress
Φ_y	energy flux in vertical direction

Subscripts

b	bulk
c	centreline
f	flat wall
m	mean
n	normal
r	riblet wall
rms	root mean square
w	wall
τ	friction value
0	at time $t = 0$

Superscripts

$+$	dimensionless length, $y^+ = u_\tau y/\nu$
$'$	fluctuating value
n	time level

displayed the highest Reynolds analogy factor, with an increase in the heat transfer coefficient of as much as 36% for the riblets with $s^+ = 16$. In a recent experimental study Choi and Orchard (1997) measured the heat transfer characteristics of triangular riblets in a thermal turbulent boundary layer. Their results indicate that the heat transfer coefficient over the riblet-covered surface is increased, from that of a smooth surface, by as much as 10% within their drag-reducing regime, and up to 30% in the drag-increasing regime of riblets. Maciejewski and Rivir (1994) investigated experimentally the effects of free-stream turbulence and surface riblets on the heat transfer rate in a linear turbine cascade. Their results seem to contradict the previous investigators, since they observed that, under certain conditions, surfaces with riblets can reduce the average heat transfer rate in the cascade by as much as 7%.

The discrepancies between different experimental investigations might be attributed to the fact that heat transfer takes place in a thin layer just above the wall, where measurement uncertainties are usually large, and to spurious effects, like lateral heat conduction and radiation heat transfer (Choi and Orchard, 1997), which are difficult to control in an experimental set-up; in addition, in some of these experimental studies, it is unclear whether the measurements were taken when the thermal development was complete.

Given these uncertainties, it is believed that numerical simulation represents a useful complement to experimental investigation, particularly in view of controlled boundary conditions and absence of side-effects, and might constitute the only available tool for subsequent geometrical optimization.

The direct numerical simulations (DNS hereafter) of the sole turbulent flow over riblets have been already performed (Choi et al., 1993; Chu and Karniadakis, 1993; Goldstein et al., 1995) and some of these numerical simulations (Choi et al., 1993; Goldstein et al., 1995)

were quite successful in reproducing the global drag reduction observed experimentally, and also in clarifying the corresponding mechanisms involved.

In the attempt to predict the thermal field in the turbulent regime, numerical analyses based on turbulence models have been performed by Launder and Li (1993) and, recently, by Benhalilou and Kasagi (1999). In the former study, a difficulty in predicting correctly even the drag variation was experienced. The latter work, based on a non-linear low-Reynolds number k–ϵ model with several turbulent heat flux representations, has shown that, by comparison of the predicted drag variation with previous experimental data, the turbulence model adopted can simulate the turbulent flow over riblets reasonably well. However, there are significant discrepancies between their heat transfer results and some of the experimental studies, since they found that the heat transfer performance can be increased, beyond that on a smooth wall, only for high Prandtl number fluids, whereas the experiments (Walsh and Weinstein, 1979; Lindemann, 1985; Choi and Orchard, 1997) indicate a significant increase for air flow.

In this study, we perform the DNS of turbulent flow and heat transfer over triangular riblets, with the objective to investigate their heat transfer effectiveness. The computational domain is a channel, where one of the walls is a plate with triangular riblets, and the opposite wall is a flat plate. Constant heat flux is assumed at both walls. The numerical algorithm adopted is based on a time-accurate, finite volume scheme previously developed for Cartesian coordinates (Nobile and Onesti, 1997; Piller and Nobile, 2002), and extended later to boundary-fitted geometries. Successful validation studies of the numerical procedure have been performed for the standard case of fluid flow and heat transfer in a parallel-plate channel, in laminar and turbulent regime, and a selection of the results will be illustrated.

The simulations of the riblet flow and heat transfer is performed for the turbulent case at a Reynolds number, based on the wall-shear velocity, $Re_\tau = 180$, and for four riblet geometries. The four configurations, with riblet spacings expressed in wall units $s^+ = 40$ and $s^+ = 20$, and ridge angle $\alpha = 45°$ and $60°$, are the same as those studied by Choi et al. (1993), and were chosen in order to better compare the turbulent flow results with available data.

The results obtained, for the global skin friction and second-order turbulence statistics, agree very well with those reported in past experimental and numerical studies (Walsh, 1982; Suzuki and Kasagi, 1994; Choi et al., 1993) and with the results of a preliminary investigation (Nobile et al., 2000) carried out on a coarser grid and a smaller domain. However, no evidence of heat transfer enhancement emerges from the simulations which, on the contrary, clearly indicate that the heat transfer coefficient, for all configurations, is significantly lower than that on a smooth wall. The predicted value of the heat transfer coefficient is in good agreement with the numerical results reported by Benhalilou and Kasagi (1999).

We finally agree with Benhalilou and Kasagi (1999) in asserting that it is hard to find physical arguments for the heat transfer augmentation over riblets at $Pr = 0.71$. We believe that other secondary effects, which were not accounted for in our simulations, might have played a significant role in the heat transfer increase observed in some experimental studies.

2. Computational domain

The flow geometry and coordinate system are illustrated in Fig. 1. The upper wall is a flat plate, whereas the lower wall is covered with riblets. Fully developed flow and thermal conditions are assumed in the streamwise direction.

The computational domain for the turbulent simulations is larger (twice larger in the spanwise direction) than the minimal flow unit of Jiménez and Moin (1991) for a Reynolds number $Re_\tau = 180$, and it is also larger (3/2 times larger in the streamwise direction and 5/4 times larger in spanwise direction) than that of the DNS study on riblets performed by Choi et al. (1993) with a second order finite difference algorithm that is comparable to our numerical method. Although we cannot claim that our results are independent of domain size

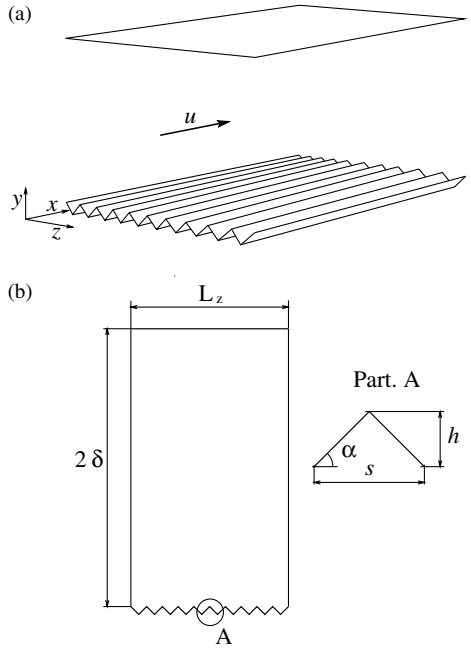

Fig. 1. Geometry of the problem: (a) three-dimensional view of the computational domain; (b) cross-sectional view.

Table 1
Parameters for the simulation of turbulent flow and heat transfer over riblets

	L_x/δ, L_y/δ, L_z/δ	$N_x \times N_y \times N_z$	α (deg)	s/δ	s^+	h/δ	h^+
Case A	1.5π, 2, 0.36125π	$33 \times 129 \times 161$	45	0.227	40.9	0.113	20.4
Case B	1.5π, 2, 0.36125π	$33 \times 129 \times 161$	60	0.227	40.9	0.197	35.4
Case C	1.5π, 2, 0.36125π	$33 \times 129 \times 321$	45	0.113	20.4	0.056	10.2
Case D	1.5π, 2, 0.36125π	$33 \times 129 \times 321$	60	0.113	20.4	0.098	17.7

and grid resolution, the adequacy of our choice is supported by the agreement of the main flow and heat transfer results with those obtained in a preliminary study (Nobile et al., 2000) on a smaller domain and a coarser grid. The detailed description of the size of the domain, mesh size, riblet spacings and ridge angles for the four configurations is displayed in Table 1. The preliminary laminar computations are carried out on the same four riblet geometries but over smaller domains, including only one riblet.

In order to assess the accuracy of the computational procedure, the plane channel in turbulent conditions is investigated, for the same values of Re_τ and Pr. The computational box for the plane channel is the same used for the riblets, with $33 \times 129 \times 65$ grid points.

3. Mathematical formulation

It is assumed that the flow is described by the three-dimensional, unsteady Navier–Stokes and energy equations with constant thermophysical properties. The equations are made dimensionless using the following reference quantities: δ, the channel half-height, for length, $u_\tau = (\tau_w/\rho)^{1/2}$ for velocity, $T_\tau = q_w/(\rho c u_\tau)$ for temperature, and $t_{ref} = \delta/u_\tau$ for time. In the preceding definitions, τ_w is the wall-shear stress and q_w is the wall heat-flux. The Reynolds number and the Prandtl number are defined as

$$Re_\tau = \frac{u_\tau \delta}{\nu}; \quad Pr = \frac{\nu}{\kappa}$$

where κ is the thermal diffusivity.

The assumption of fully developed flow and heat transfer implies that the pressure and temperature fields can be expressed as the sum of a fluctuating periodic component, and a linear gradient:

$$p^* = p - \left|\frac{\mathrm{d}\overline{p^*}}{\mathrm{d}x}\right| x \tag{1}$$

$$T^* = T + \left|\frac{\mathrm{d}\overline{T^*}}{\mathrm{d}x}\right| x \tag{2}$$

where the pressure gradient is given, from a force balance, by

$$\left|\frac{\mathrm{d}\overline{p^*}}{\mathrm{d}x}\right| = \rho u_\tau^2/\delta \tag{3}$$

and the temperature gradient is given, from an energy balance, by

$$\left|\frac{\mathrm{d}\overline{T^*}}{\mathrm{d}x}\right| = \frac{q_w}{\rho c u_b \delta} \tag{4}$$

In Eqs. (1)–(4) the overbar indicates time averaged quantities. With the chosen set of reference quantities, and using Eqs. (1) and (2), the non-dimensional governing equations for mass, momentum and energy are

$$\nabla \cdot \mathbf{u} = 0 \tag{5}$$

$$\frac{\partial \mathbf{u}}{\partial t} + (\mathbf{u} \cdot \nabla)\mathbf{u} = -\nabla p + \frac{1}{Re_\tau}\nabla^2 \mathbf{u} + \mathbf{x} \tag{6}$$

$$\frac{\partial T}{\partial t} + \mathbf{u} \cdot \nabla T + \frac{u}{u_b} = \frac{1}{Re_\tau Pr}\nabla^2 T \tag{7}$$

where u_b is the bulk (mean) velocity, the last term on the right-hand side of Eq. (6) represents the imposed pressure gradient in the streamwise direction, and the last term on the left-hand side of Eq. (7) takes into account the linear streamwise temperature gradient, expressed by Eq. (4). Periodic boundary conditions are applied for velocity, pressure and temperature, in the streamwise (x) and spanwise (z) directions. No-slip conditions are enforced at the walls, together with constant heat flux, and thus the wall temperature is allowed to fluctuate. Due to the homogeneity of the flow and temperature fields in the streamwise and spanwise directions, within a periodic length equal to the half-width of the riblet, all the relevant quantities are obtained by first averaging along x and time. The average is then performed over all the riblets, and once more across the riblet centreline.

3.1. Heat transfer parameters

The heat transfer rate, for both flat and riblet walls, is evaluated through the Nusselt and Stanton numbers, which, in terms of dimensionless quantities, become:

$$Nu = \frac{4 Re_\tau Pr}{(T_w - T_b)} \tag{8}$$

$$St = \frac{1}{u_b (T_w - T_b)} \tag{9}$$

We point out that, since the surface modification by riblets has a similar size to that of surface roughness, we compare the forces applied at the two walls, irrespective of the different surface of application, and that the heat flux imposed on the projected surfaces is the same. This is a common practice among other authors (Walsh and Weinstein, 1979; Choi and Orchard, 1997).

In order to evaluate the heat transfer effectiveness of the riblet surface, we make use, in agreement with Benhalilou and Kasagi (1999), of the heat transfer efficiency of the surface, defined as

$$\eta = \frac{(2St_r/D_r)}{(2St_f/D_f)} \tag{10}$$

where the subscripts 'r' and 'f' refer to the riblet and flat wall, respectively, and D represents the non-dimensional averaged drag force on the wall:

$$D = \int_A \left.\frac{\partial u}{\partial n}\right|_w \mathrm{d}A \tag{11}$$

where n is the coordinate normal to the surface, and A denotes the wetted area of the surface and u the streamwise velocity component, all these quantities being dimensionless. The comparison between the flat wall values and the values computed on the wall with riblets relies upon the assumption that the turbulent flow near one wall of the channel does not affect the skin friction and heat transfer at the other (Choi et al., 1993).

4. Numerical methods

In this section, a summary of the numerical procedure is presented. The Navier–Stokes and energy equations (5)–(7) are solved by a second order projection scheme, as proposed by Gresho (1990); the numerical integration from the time instant $t^{(n)}$ to $t^{(n+1)} = t^{(n)} + \Delta t$, involves the following steps:

1. Calculation of the new temperature field:

$$\frac{T^{(n+1)} - T^{(n)}}{\Delta t} = -\frac{1}{2}\left[3(\mathbf{u}\cdot\nabla T)^{(n)} - (\mathbf{u}\cdot\nabla T)^{(n-1)}\right] + \frac{1}{2Re_\tau Pr}\left(\nabla^2 T^{(n+1)} + \nabla^2 T^{(n)}\right) - \frac{u^{(n)}}{u_b^{(n)}} \tag{12}$$

2. Calculation of the intermediate velocity field $\tilde{\mathbf{u}}^{(n+1)}$:

$$\frac{\tilde{\mathbf{u}}^{(n+1)} - \mathbf{u}^{(n)}}{\Delta t} = -\frac{1}{2}\left[3(\mathbf{u}\cdot\nabla)\mathbf{u}^{(n)} - (\mathbf{u}\cdot\nabla)\mathbf{u}^{(n-1)}\right] + \frac{1}{2Re_\tau}\left(\nabla^2\mathbf{u}^{(n+1)} + \nabla^2\mathbf{u}^{(n)}\right) - \nabla p + \mathbf{x} \tag{13}$$

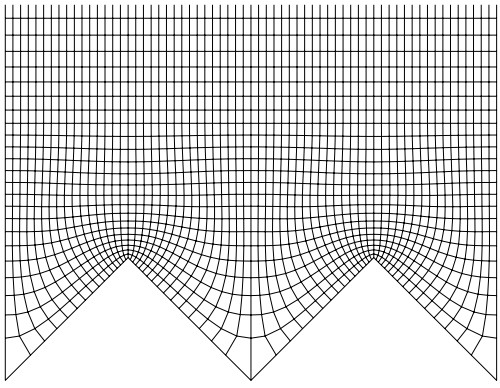

Fig. 2. Computational mesh near the $\alpha = 45°$ riblets.

Table 2
Results for the laminar simulations

	D_r/D_f	St_r/St_f	η	Nu_r	Nu_f
Plane channel					
Present	1.000	1.000	1.000	–	8.233
Analytical (Bhatti et al.)	–	–	–	–	8.235
FEM, 6 refinements	1.000	1.000	1.000	–	8.235
Case A					
Present	1.0260	0.9554	0.9312	7.9628	8.3344
FEM, 8 refinements	1.0252	0.9533	0.9298	7.9481	8.3379
Case B					
Present	1.0662	0.8989	0.8431	7.6219	8.4793
FEM, 9 refinements	1.0601	0.8931	0.8424	7.5771	8.4845
Case C					
Present	1.0130	0.9765	0.9640	8.0895	8.2839
FEM, 8 refinements	1.0132	0.9754	0.9627	8.0833	8.2867
Case D					
Present	1.0328	0.9459	0.9159	7.9036	8.3554
FEM, 8 refinements	1.0292	0.9428	0.9160	7.8807	8.3589

3. Calculation of the auxiliary variable ϕ from the Poisson equation:

$$\nabla^2\phi = \nabla\tilde{\mathbf{u}}^{(n+1)} \tag{14}$$

with $\partial\phi/\partial n = 0$ at all wall boundaries, where n is the coordinate normal to the wall.

4. Update, by projection, of the tentative velocity $\tilde{\mathbf{u}}^{(n+1)}$, in order to obtain a divergence free velocity field $\mathbf{u}^{(n+1)}$ from the relation:

$$\mathbf{u}^{(n+1)} = \tilde{\mathbf{u}}^{(n+1)} - \nabla\phi \tag{15}$$

5. Computation of the new pressure field at $t^{(n+1)}$ from:

$$p^{(n+1)} = p^{(n)} + \frac{\phi}{2\Delta t} \tag{16}$$

In Eqs. (12) and (13), temporal discretization is done with the Crank–Nicolson scheme on the viscous term, and the Adams–Bashfort scheme for the convective term. Eqs. (12)–(14) are integrated by a finite volume method on a underlying orthogonal boundary fitted grid in the y–z plane, and a uniform Cartesian discretization in the streamwise x direction, the velocity components u, v and w being evaluated on an auxiliary staggered mesh. The detailed $\alpha = 45°$ computational mesh near the riblets, in the cross-flow plane, is illustrated in Fig. 2. The variable values and the spatial derivatives at the cell faces are computed using second order central difference relations.

The transport equations (12) and (13) are solved by the approximate factorization method, while the time-consuming pressure Poisson equation (14), which arises at every time-step, is solved by a fast Poisson solver, based on FFT decomposition along the x (streamwise) direction and block Gaussian elimination (Ghia and Ghia, 1988) in the decoupled y–z planes. Accordingly, the procedure is second order accurate in both time and space. A more detailed description of a similar numerical algorithm, although on a Cartesian grid, can be found in a DNS study of turbulent heat transfer in a square duct (Piller and Nobile, 2002).

The CPU time per time-step for the larger case C and case D grid is about 16 s, on a single Power 4 1300 MHz processor of an IBM SP4.

The initial conditions for the velocity field are obtained from the correlation for the mean turbulent velocity profile (Bhatti and Shah, 1987), by superimposing random fluctuations on the cross-flow velocity components; the initial conditions for the temperature are derived from the streamwise velocity initial field through Eq. (17):

$$T_0 = -Pr \cdot u_0 \tag{17}$$

After about 100 time units (δ/u_τ), when a statistical steady-state is reached, the integration continues in order to sample time-averaged local and global quantities. The sampling time for the four cases is between 35 and 36 time units, during which a realization of the flow and temperature field is stored every $0.1\delta/u_\tau$. We observed that, due to the limited size of the domain, this sampling time is barely sufficient to discriminate the variations in some global quantities, like the ratio of the drag of the riblet-covered surface to that of the smooth wall. After averaging, the remaining fluctuations are about $\pm 2\%$ for the friction factor and the Stanton number. Therefore, the error bound for the statistical sampling error is estimated to be of the order of $\pm 2\%$.

5. Results and discussion

5.1. Laminar cases

The laminar simulations have been carried out on the same four riblet geometries of the turbulent cases, whose riblet spacing s/δ and ridge angle α are specified in Table 1. These simulations have been conducted in order to

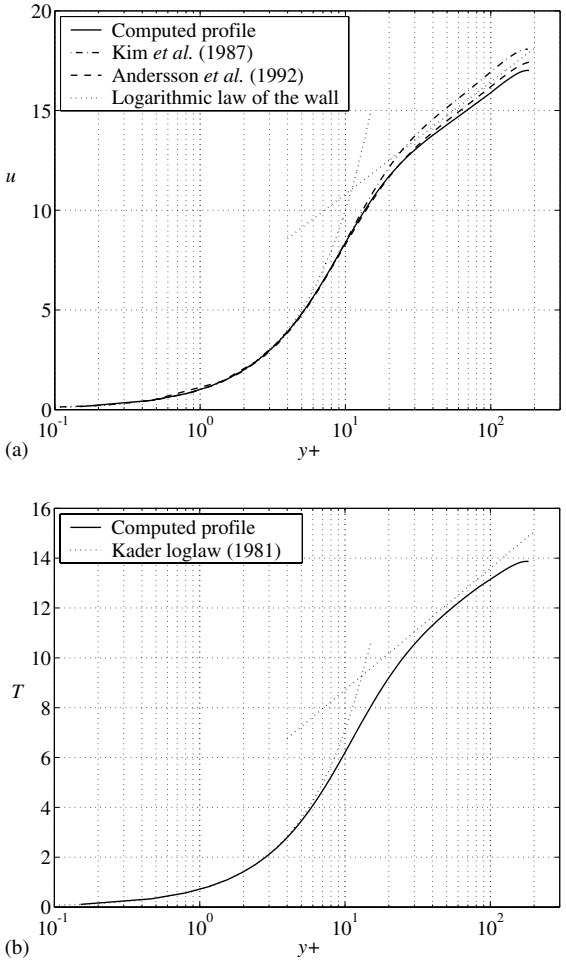

Fig. 3. Turbulent flow in a plane channel at $Re_\tau = 180$: (a) mean velocity profile; (b) mean temperature.

first check the numerical accuracy of our procedure, and to estimate the heat transfer performance of riblets in the steady, laminar regime.

The calculations have been performed using the same computer code we have developed for DNS together with a simpler, but more accurate, approach based on a two-dimensional model implemented via the FEMLAB finite element package (Femlab Reference Manual, 1999). In the latter implementation, only a pair of two-dimensional Poisson equations are solved, since equations (5)–(7), in the case of fully developed laminar flow in channels, reduce to:

$$\frac{\partial^2 u}{\partial y^2} + \frac{\partial^2 u}{\partial z^2} = -Re_\tau \tag{18}$$

$$\frac{\partial^2 T}{\partial y^2} + \frac{\partial^2 T}{\partial z^2} = Re_\tau Pr \frac{u}{u_b} \tag{19}$$

The calculations with the DNS code are carried out for $Re_\tau = 10$ which corresponds to a Reynolds number $Re_{4\delta} \approx 133$, based on the mean velocity and twice the height of the channel, and for a Prandtl number $Pr = 0.71$; these data are however just a requirement of the solver, since it is well known that the results, in fully developed laminar regime, are independent of Re_τ and Pr.

The resolution in spanwise and wall normal directions for the laminar simulations is the same as the turbulent case, but the domain includes only one riblet, thus reducing the number of cells in the spanwise direction to 32; four cells are used in the streamwise direction. In the two-dimensional unstructured FEM approach, the equations are solved using the adaptive-grid strategy provided by FEMLAB, which led to results that were independent of further grid refinements to better than 0.1% of the computed values, using up to 1.2×10^5 grid points.

All the laminar results are reported in Table 2. The value of Nu obtained on the parallel plane-channel with uniform heat flux at both walls differs by less than 0.03% from the analytical value (Bhatti and Shah, 1987). Over riblets, the agreement between our results and those obtained with FEMLAB can be considered very good, with maximum differences of 0.6% for the drag ratio and the heat transfer coefficient, and an average error of 0.3%.

The results indicate, in agreement with Choi et al. (1991), that the riblets present an increased drag in laminar flow, and that the drag is higher for the larger riblets; moreover the drag is higher over the sharper riblets. The Nu value is smaller over the grooved walls, and this reduction is larger for the $s^+ = 40$ riblets; for a fixed value of riblet spacing, the difference between the Nusselt number on the two walls is twice larger on the $\alpha = 60°$ riblets. The increase in drag, together with the decrease in heat transfer coefficient, lead in turn to a significant decrease of the efficiency η, particularly for the larger and sharper case B riblets.

5.2. Turbulent flow in a plane channel

The simulation of the turbulent flow and heat transfer in a plane channel has provided a mean to check the accuracy of our code in performing the DNS at a Rey-

Table 3
Overall results for the turbulent simulations, at $Re_\tau = 180$ and $Pr = 0.71$

	D_r/D_f	St_r/St_f	η	Nu_r	Nu_f
Plane channel					
Present	1.00	1.00	1.00	–	40.5
Correlation (Bhatti et al.)	–	–	–	–	39.3
Case A					
Present	1.05	0.89	0.84	35.1	39.6
Exp. (Walsh)	1.03	–	–	–	–
DNS (Choi et al.)	1.02	–	–	–	–
Case B					
Present	1.13	0.78	0.69	30.5	38.9
Exp. (Walsh)	1.11[a]	–	–	–	–
DNS (Choi et al.)	1.12	–	–	–	–
Case C					
Present	0.99	0.88	0.89	35.6	40.3
Exp. (Walsh)	0.98	–	–	–	–
DNS (Choi et al.)	0.95	–	–	–	–
Case D					
Present	0.98	0.74	0.75	30.4	40.8
Exp. (Walsh)	0.96[a]	–	–	–	–
DNS (Choi et al.)	0.94	–	–	–	–

[a] Denotes data obtained from the case $s^+ = h^+$, that is $\alpha \approx 63°$.

nolds number $Re_\tau = 180$, equivalent of about $Re_{4\delta} = 12 \times 10^3$, on a domain with the same dimensions and the same number of grid points in the streamwise and wall normal directions as the ribbed channels, but with only 65 grid points in the spanwise direction.

The velocity profile, illustrated in Fig. 3, is compared with the law of the wall $u = 5.2 + \ln y^+/0.41$, with the results from a finite difference, 129^3 grid points, simulation (Andersson and Kristoffersen, 1992), and with the profile from the spectral DNS by Kim et al. (1987) that better represents the low Reynolds flow features. The agreement between our results and the other data can be deemed reasonable.

The absolute value of the temperature difference between the wall and the fluid is compared in Fig. 3 with the Kader log-law (Kader, 1981), obtained from experimental data and which, for $Pr = 0.71$, gives $T = 3.83 + 2.12 \ln y^+$. As can be observed, the agreement between our results and this empirical law is quite satisfactory.

All the fluid flow results, together with the second order statistics illustrated in the following section, though obtained with a rather coarse grid and a limited domain, agree sufficiently well with the reference data and with the logarithmic law of the wall; the same level of accuracy is achieved for the main heat transfer characteristics, like the Nusselt number that is compared in Table 3 with the value provided by an experimental correlation (Bhatti and Shah, 1987).

5.3. Turbulent flow over riblets

5.3.1. Mean secondary flow

The calculation of turbulent flow above riblets reveals the presence of mean secondary flows, which consist of matched pairs of streamwise vortices that are not sustained in a fully developed laminar flow of the same geometry.

The turbulent cross-flow mean velocities are illustrated in Fig. 4, where the upward motion above the peak, and the downward flow towards the valley, is evident and in agreement with the experimental findings of Suzuki and Kasagi (1994), and the DNS study of Choi et al. (1993).

The maximum intensity of the mean secondary velocities in the drag reducing case D is 0.2% of the centreline velocity, while in the drag increasing case B it represents the 0.7% of the maximum streamwise velocity; these values almost coincide with the results of the DNS of Choi et al. (1993) who calculated values of 0.2% and 0.8%, respectively, on the same geometries and match very well the measured values by Suzuki and Kasagi (1994), despite some differences in riblet configuration. In the $s^+ = 40$, $\alpha = 45°$ case A we find one more pair of weaker, counter-rotating vortices in the riblet valley, clearly visible in Fig. 4.

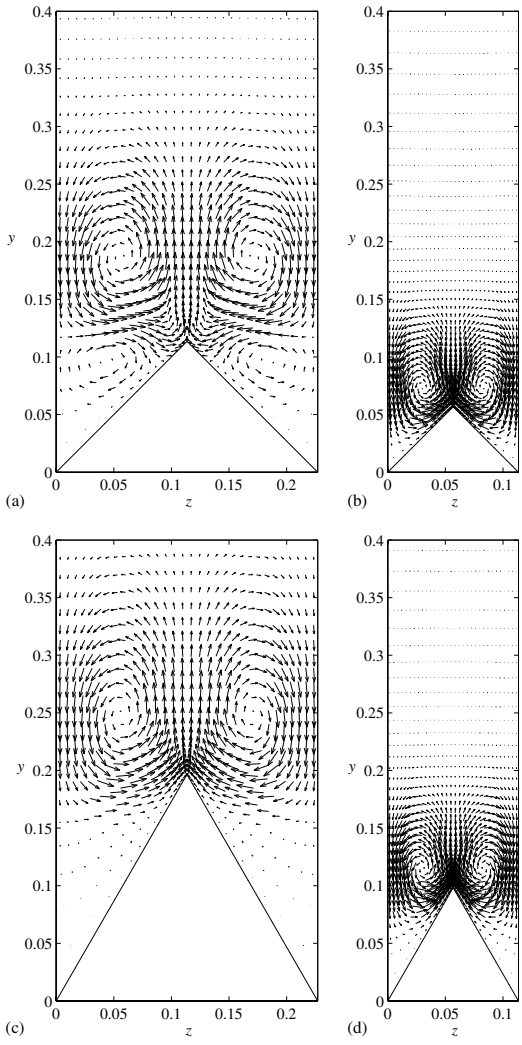

Fig. 4. Mean secondary flow above riblets: (a) case A; (b) case C; (c) case B; (d) case D.

5.3.2. Turbulence intensities

The root mean square velocity fluctuations across the channels with $\alpha = 60°$ riblets, are depicted in Fig. 5. We obtained, in agreement with the experiments of Suzuki and Kasagi (1994) and the Choi et al. (1993) computations, that in the drag-reducing configurations the peak values of the root mean square of all velocity components are decreased by about 5% compared with the flat side values; this is also true in comparison with the plane channel results.

In the drag augmenting configuration case B, the maximum in u_{rms} is 15% smaller than the flat side value above the riblet valley, but reaches the same values over the riblet tip. Vice versa the peaks of v_{rms} and w_{rms} are higher, 7% and 10% respectively, over the grooves. It should be noticed in Fig. 5 that the root mean square values in the $s^+ = 40$ case B are decreased on the flat side besides being increased over the riblets.

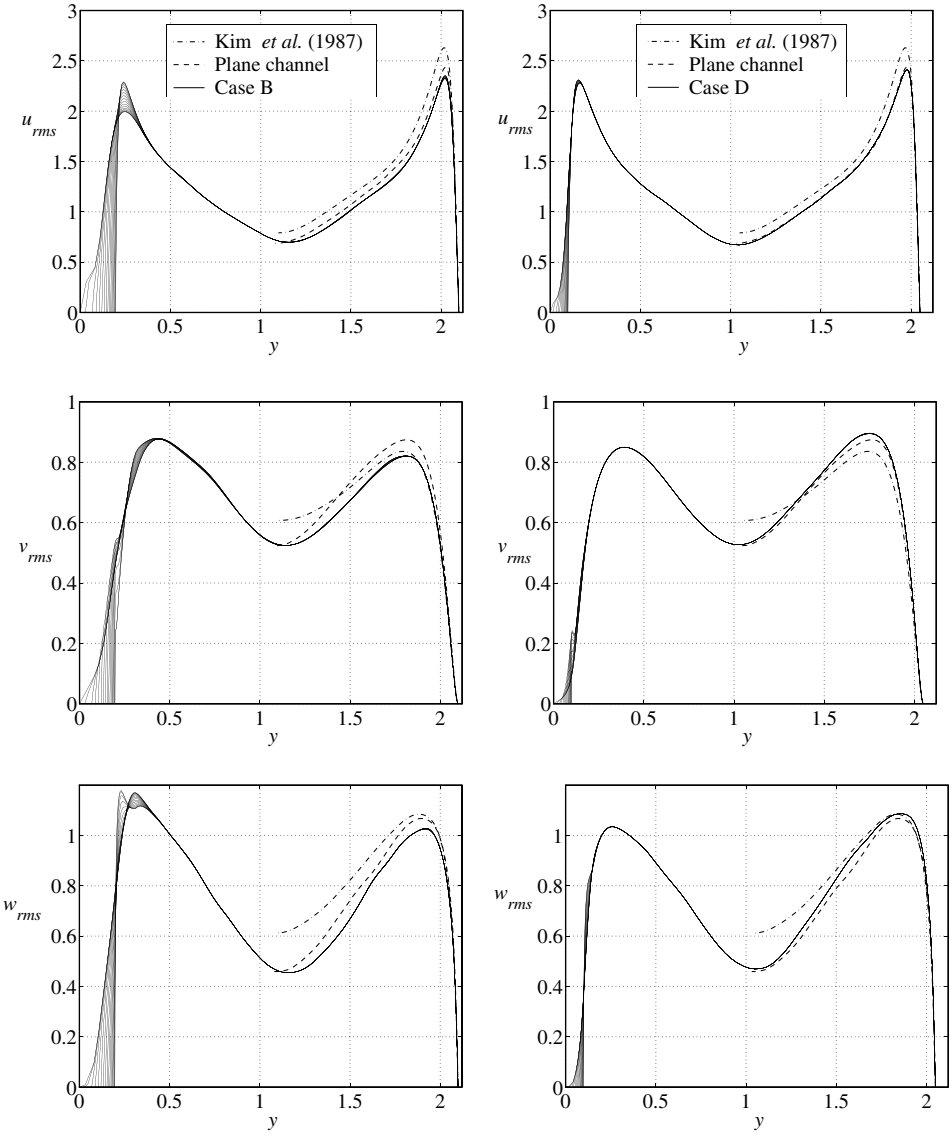

Fig. 5. The three components of the turbulence intensity: left, case B; right, case D. The figures show the comparison of the plane channel results and the Kim et al. (1987) computations with the smooth wall side values.

The location of the maximum streamwise turbulence intensity above the riblet tips is always closer to the wall than what happens for the flat plate, whereas the locations of the peaks above the riblet valleys are further away from the wall; this trend, observed also by Choi et al. (1993), is clear from Fig. 6 for the $\alpha = 45°$ case A and case C, where the variable y_w represents the vertical distance from the solid wall.

5.3.3. Reynolds shear stress

The Reynolds shear stress $-\overline{u'v'}$ is shown in Fig. 7 as a function of the vertical distance y_w from the solid wall. In the drag decreasing case D, the maximum Reynolds stress above the riblets is reduced by 8%, while in the drag increasing case B it is significantly increased, up to 24%, over the riblet tip, and remains unaltered above the riblet valley.

The amount of reduction of velocity fluctuations, and particularly the decrease of the Reynolds stress near the drag decreasing riblets are, in our computation, very similar to the DNS results of Choi et al. (1993) and the values measured by Suzuki and Kasagi (1994).

The decrease of the Reynolds stress over the $s^+ = 20$ riblets, where there are no considerable variations in the mean velocity field in comparison with the flat channel, confirm the measured drag reducing features of the small riblets.

5.3.4. Mean velocity and temperature

The velocity and temperature profiles in the logarithmic region are depicted in Fig. 8, where they are also

compared with the results for the plane channel. Caution should be exercised when judging these plots, since they are made using the riblet midpoint as $y = 0$ for both velocity and temperature plots, while it is well known (Baron et al., 1989; Choi et al., 1993) that a *virtual origin*, defined as the location of an *imaginary flat surface* which matches the riblet velocity profile above the viscous sublayer, should be more appropriate, though there is no general consensus about the proper evaluation of the virtual origin. Furthermore in these plots the temperature was changed in sign and the zero mean value was assigned to the riblet mid height.

The figure shows that the slope of the mean velocity profiles above the viscous sublayer is similar to that of the flat channel, although there is a clear upward shift of the $s^+ = 20$ case C and case D velocity profiles, in comparison with the $s^+ = 40$ cases. This shift is an indication of the increase of the viscous sublayer thickness (Choi et al., 1993), and results in a net drag reduction.

The temperature plots in Fig. 8 are even more meaningful since for all configurations, no matter whether the origin is located in the valley, tip or mid-height of the riblet, the mean temperature profiles are well above the flat channel values, while maintaining the same slope. This is a clear indication of a thickening of the conduction sublayer, which in turn leads to a reduction of the heat transfer coefficient.

5.3.5. Drag and heat transfer

The case A time history of the drag ratio, Stanton ratio and overall efficiency is shown in Fig. 9. An intermittent behaviour of such global quantities, due to the limited size of the computational domain, is observed. The large amplitude and period of the oscillations justifies the requirement of a long sampling time for the proper evaluation of the drag and the heat transfer rate. However, it is evident from the same Fig. 9, that the Stanton ratio St_r/St_f, and consequently the

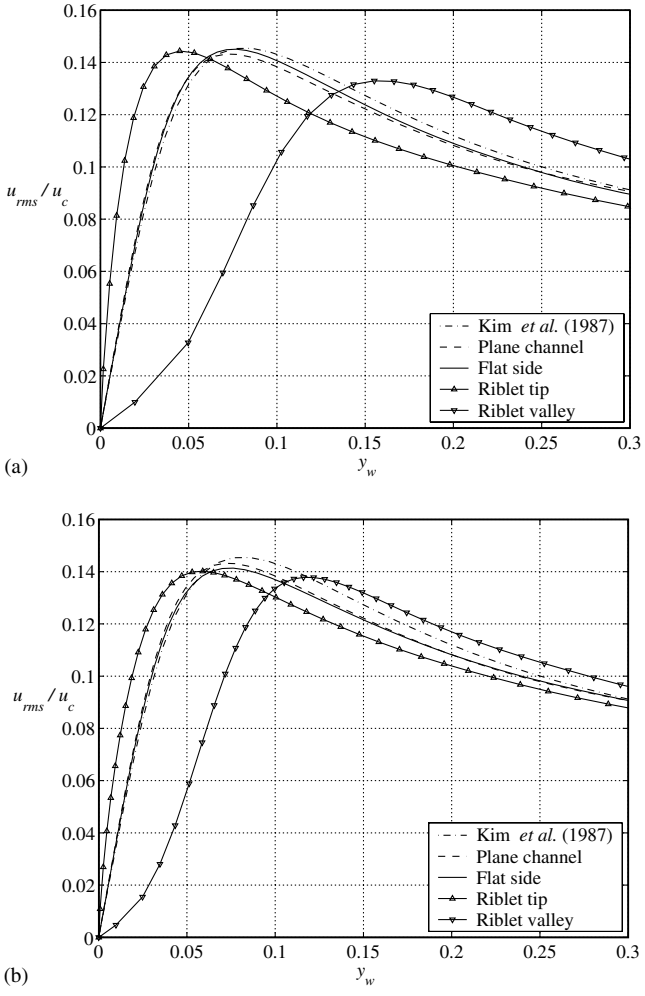

Fig. 6. Streamwise component of the turbulence intensity normalized by the centreline mean velocity, as a function of the vertical distance from the wall y_w: (a) case A; (b) case C.

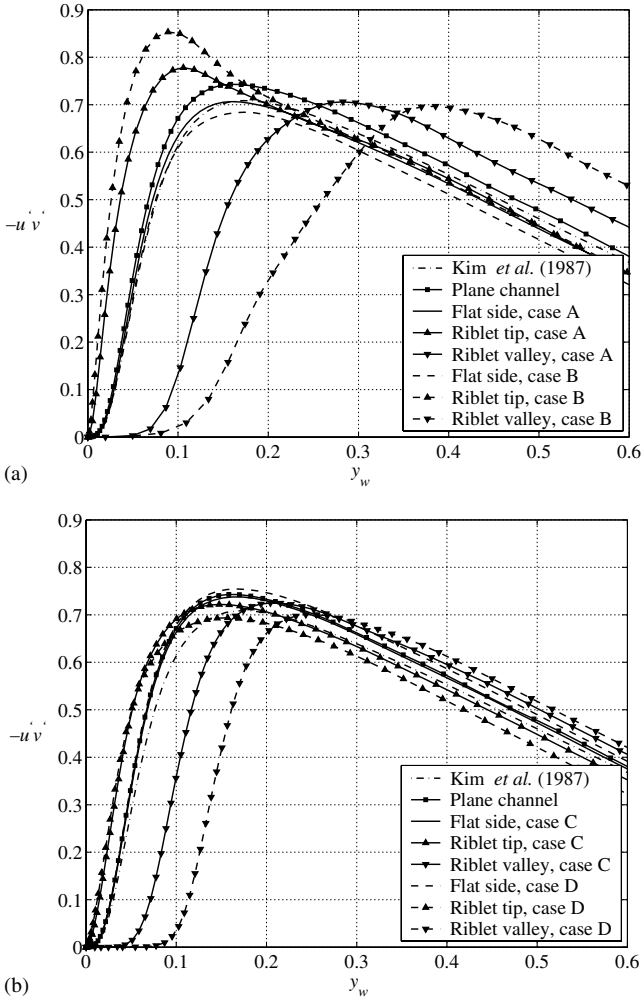

Fig. 7. Reynolds shear stress: (a) case A and case B; (b) case C and case D. The figure also compares the results with the Kim et al. (1987) computation.

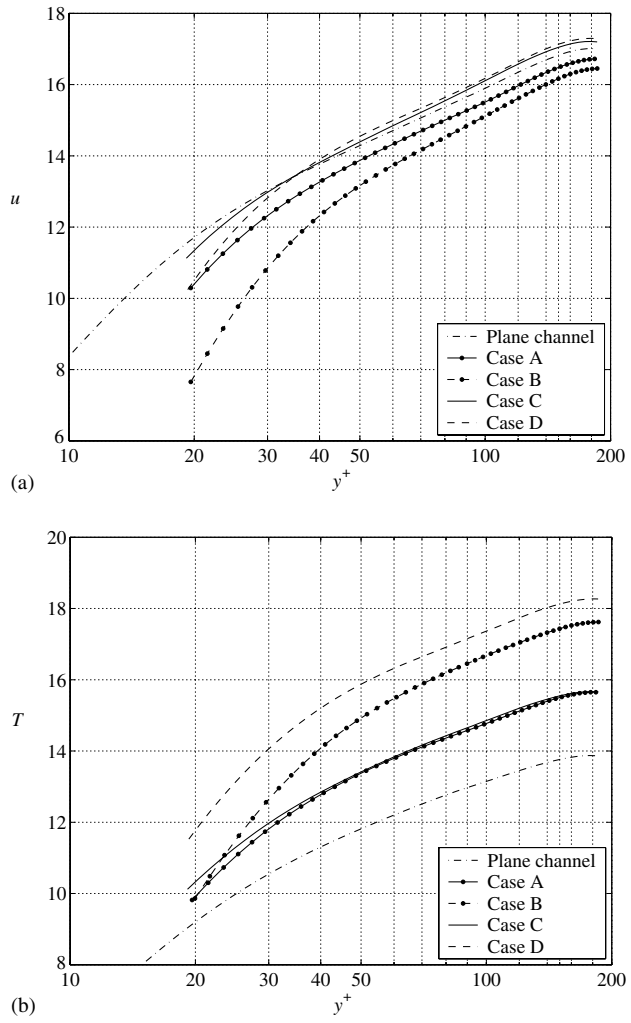

Fig. 8. Turbulent flow above riblets at $Re_\tau = 180$ and $Pr = 0.71$: (a) mean velocity profiles; (b) mean temperature.

heat transfer efficiency η, are almost constantly less than one, even in the case of highest time averaged Stanton ratio. The resulting time and space averages of the global quantities, performed in a time interval of more than $35\delta/u_\tau$, for each turbulent case, are reported in Table 3.

The predicted values of the drag-ratio are in good agreement with past experimental (Walsh, 1982) and DNS (Choi et al., 1993) results, since, as already observed, a 2% error on the evaluation of this quantity is expected as a consequence of the limited sampling time and domain.

The Nusselt number values evaluated at the riblet wall Nu_r, are all lower than Nu_f, with differences between 11% and 25%, for case A and case D, respectively. The Stanton ratio values are well below one in all configurations. These results indicate, within the limitation due to the low value of Reynolds number that we consider, that there is certainly no heat transfer augmentation over riblets for $Pr = 0.71$.

It is difficult to try to explain the reasons of the discrepancy between our numerical results and some of the experimental studies (Walsh and Weinstein, 1979; Choi and Orchard, 1997), where a net heat transfer increase was observed on riblet-mounted surfaces, for the same Pr value. These discrepancies might be partially attributed to the difficulty of the measurements near the small grooves, and to spurious effects, like lateral heat conduction and radiation heat transfer, but the magnitude of the differences suggests that other causes should be involved. Possibly the measurements were conducted at an intermediate stage of the thermal development, when the layer is thinner and favourable heat transfer coefficients are likely to be measured.

On the other hand our results agree well with the main conclusions of the numerical work of Benhalilou and Kasagi (1999), which found that, for ribbed chan-

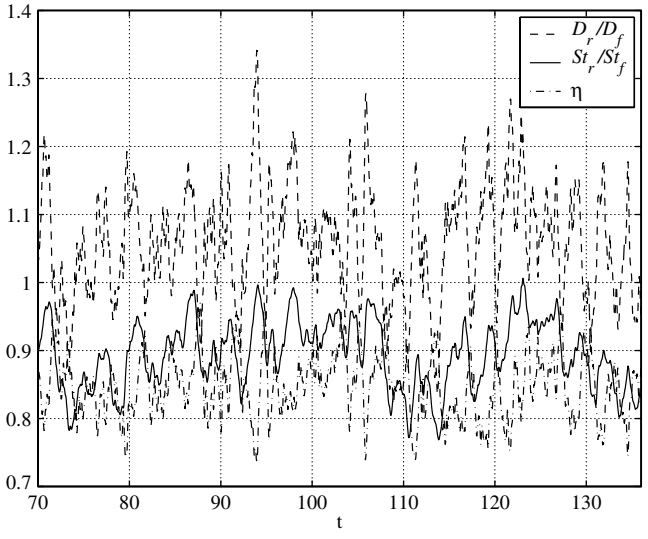

Fig. 9. Time history of the drag ratio D_r/D_f, Stanton ratio St_r/St_f, and heat transfer efficiency η for the case A configuration.

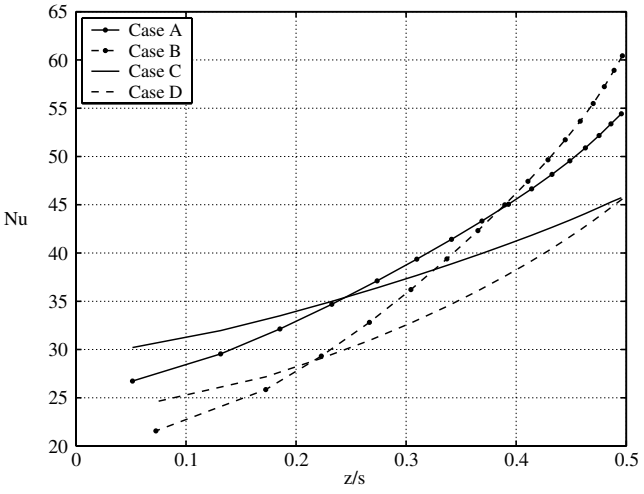

Fig. 10. Local Nu number on the riblet wall as a function of the spanwise position z/s along the riblets.

nels, the heat transfer performance can be increased, beyond that on a smooth wall, only for high Prandtl number fluids.

We remark, in support of the conclusions drawn here, that the $\alpha = 45°$ cases were investigated in a preliminary study (Nobile et al., 2000) where the main findings like the drag-ratio, the Stanton number ratio and overall efficiency were calculated on coarser grids, of about one fifth of the present grid points, and on an almost twice smaller domain. The results differ by no more than 2% from the present ones, and the difference in Nusselt number is below 5%. Considering the extent of the reduction in the heat transfer coefficients we believe that the main conclusions of this study, i.e. the heat transfer decrease on $s^+ = 20$ and $s^+ = 40$ riblets at low Reynolds number for a $Pr = 0.71$ fluid, can hardly be questioned.

5.3.6. Conditions for heat transfer enhancement

In this section we try to analyse the conditions that can lead to heat transfer enhancement, compared to the flat plate, of riblets. The aim is to look for the conditions under which the difference between the mean temperature at the riblet wall and the bulk temperature, ΔT_r, decreases in comparison with the equivalent on the flat wall ΔT_f. In particular, under a drag reducing regime, and under the assumption of no variations of the flow field, a positive value of the difference between the two temperature drops $\Delta T_{fr} = \Delta T_f - \Delta T_r > 0$ implies a favourable efficiency value $\eta > 1$.

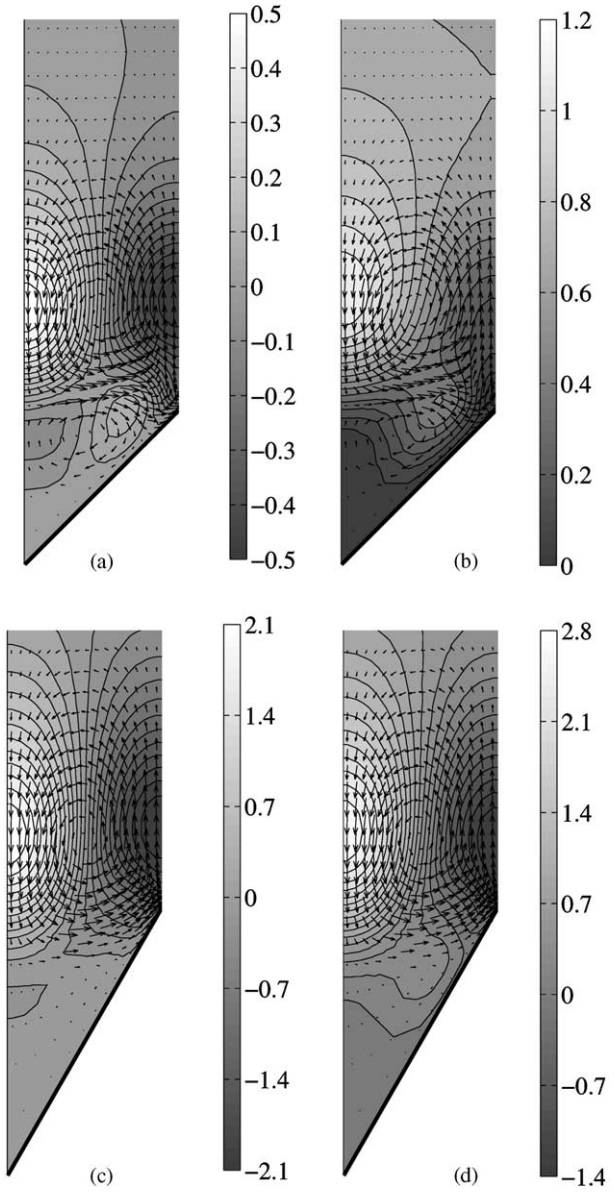

Fig. 11. Mean advective vertical heat flux $\bar{v}\bar{T}$ with superimposed vectors of mean secondary flow: (a) case A; (c) case B. Total advective vertical heat flux $\bar{v}\bar{T} + \overline{v'T'}$ with superimposed vectors of mean secondary flow: (b) case A; (d) case B.

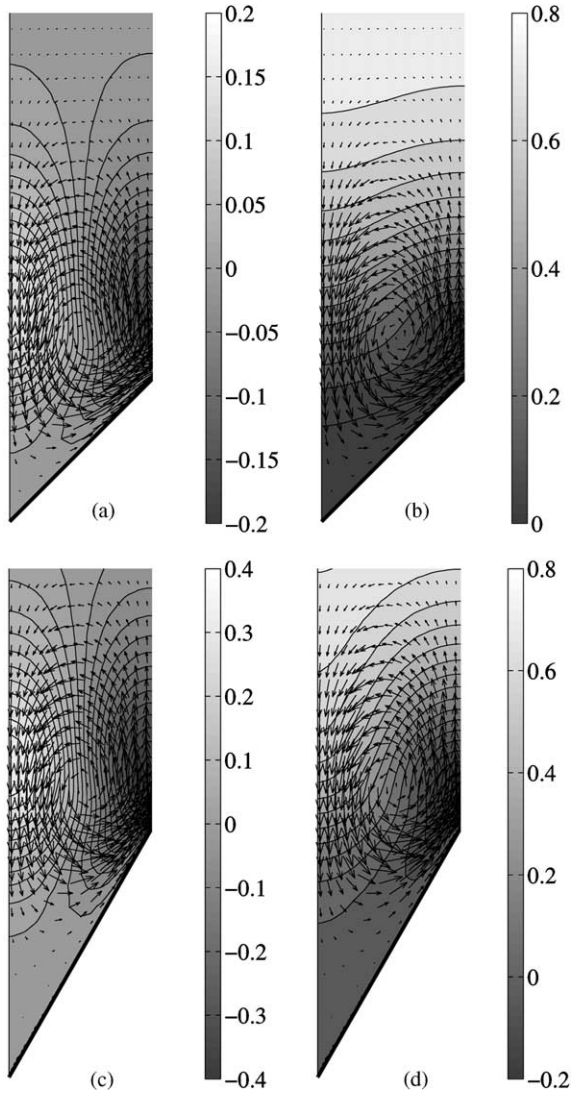

Fig. 12. Mean advective vertical heat flux $\bar{v}\bar{T}$ with superimposed vectors of mean secondary flow: (a) case C; (c) case D. Total advective vertical heat flux $\bar{v}\bar{T} + \overline{v'T'}$ with superimposed vectors of mean secondary flow: (b) case C; (d) case D.

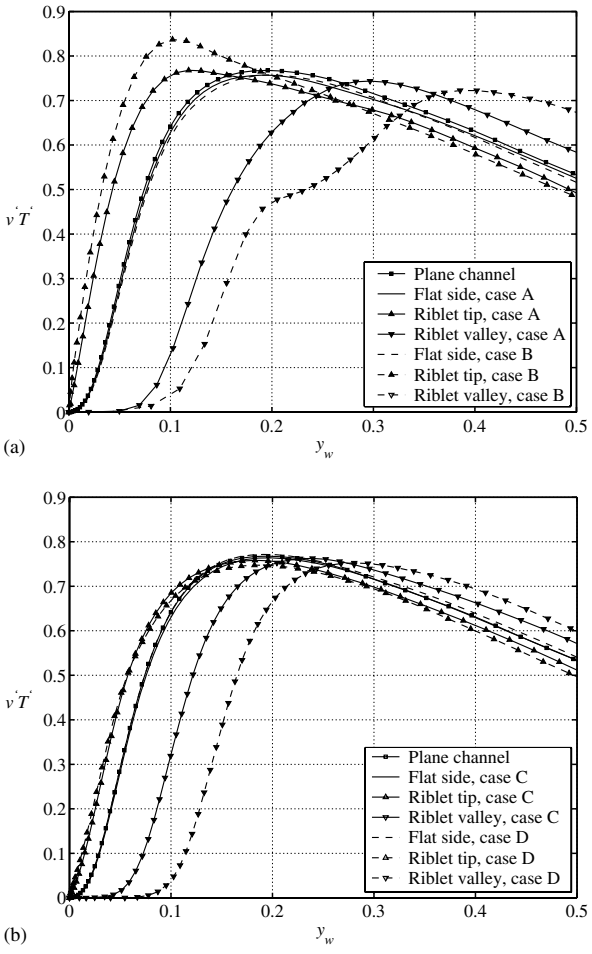

Fig. 13. Turbulent wall normal heat flux as a function of the vertical distance from the wall y_w.

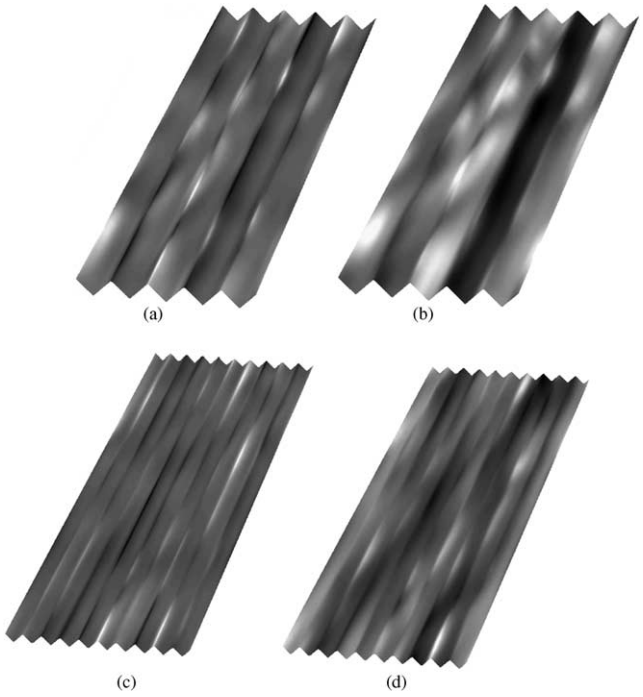

Fig. 15. Instantaneous drag and temperature fluctuations contours at the solid surfaces for case A and case C: (a) and (c) drag fluctuation; (b) and (d) temperature fluctuation. Bright spots correspond to drag and heat transfer increase.

In our computations, where a low heat transfer coefficient is predicted for both geometries, the temperature difference value ΔT_{fr} is always less than zero. In what follows we try to analyze, leaving the flow field quantities constant over the fixed geometry, if an in-

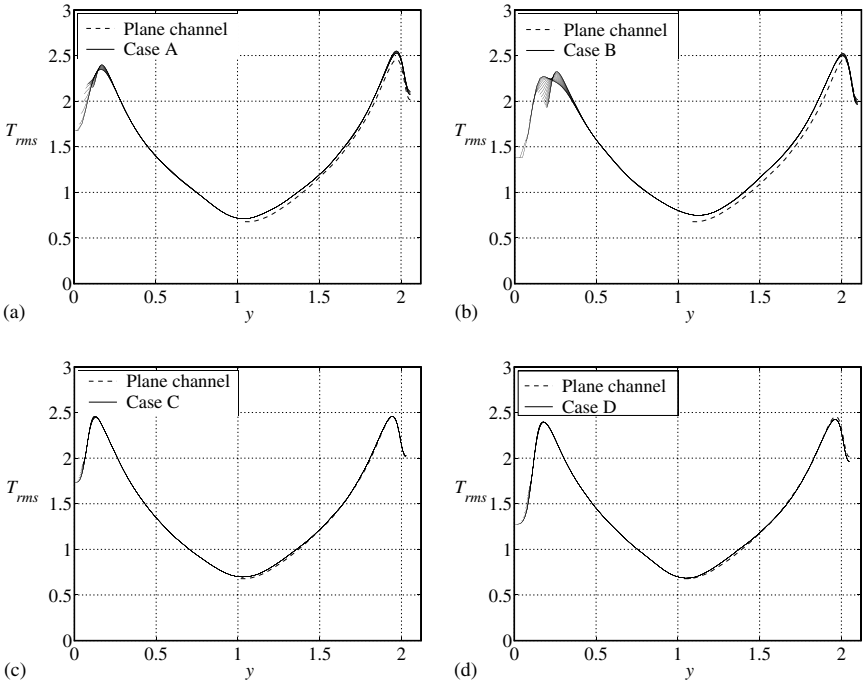

Fig. 14. Temperature root mean square: (a) case A; (b) case B; (c) case C; (d) case D. The comparison with the plane channel results is shown.

crease of the Prandtl number can possibly change the sign of the difference between the two temperature drops, as already reported by Benhalilou and Kasagi (1999).

The contribution of each term of the time-averaged energy flux $\overline{\Phi}_y$ in the y direction will be analysed separately:

$$\overline{\Phi}_y = -\frac{1}{RePr}\frac{\partial \overline{T}}{\partial y} + \overline{v}\overline{T} + \overline{v'T'} \tag{20}$$

As a consequence of the thickening of the conductive sublayer there is only a small area near the tip of the riblet, as is shown in Fig. 10, where the local Nusselt number is greater than the flat plate value, $Nu_f \approx 40$; a large reduction of the thermal layer thickness can enhance the contribution of the thermal diffusion term $-(RePr)^{-1}\partial\overline{T}/\partial y$ to the heat flux in the zone near the middle height of the riblet.

The mean advective enthalpy flux in vertical direction $\overline{v}\overline{T}$ takes into account the important effect of fluid transport from the riblet tip towards the centre of the channel, and from the core of the flow towards the wall in the valley. It is represented for the four cases in Figs. 11a, 11c, 12a and 12c; the mean value is approximately zero but the positive and negative peaks reach different values depending on the position and the intensity of the longitudinal vortices. It is unclear whether the contribution of the mean advective term $\overline{v}\overline{T}$ to heat transfer would increase for a higher Prandtl number fluid.

The turbulent vertical heat flux $\overline{v'T'}$ is depicted in Fig. 13; only small variations of $\overline{v'T'}$ between the riblet and the flat wall curves can be observed for all cases except for case B where a higher peak on the riblet tip and very low values over the valley are observed. The temperature fluctuations, reported in Fig. 14, and all the velocity

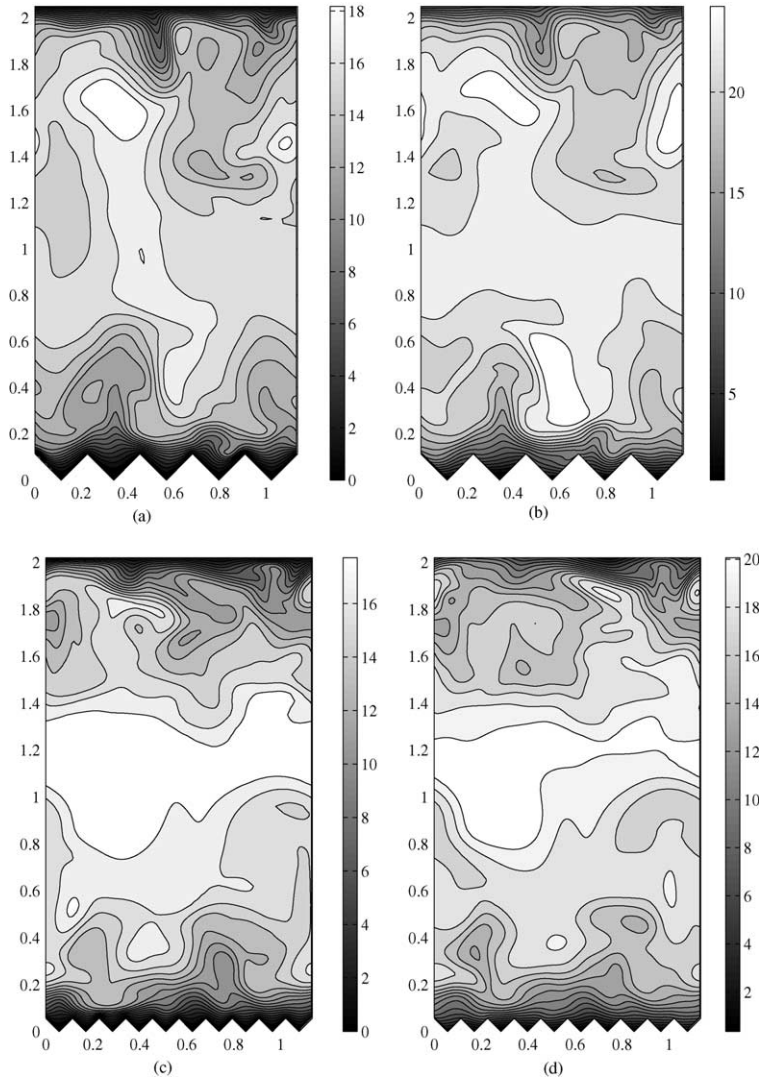

Fig. 16. Instantaneous streamwise velocity and the absolute value of the temperature difference with the flat wall for case A and case C: (a) and (c) streamwise velocity; (b) and (d) temperature.

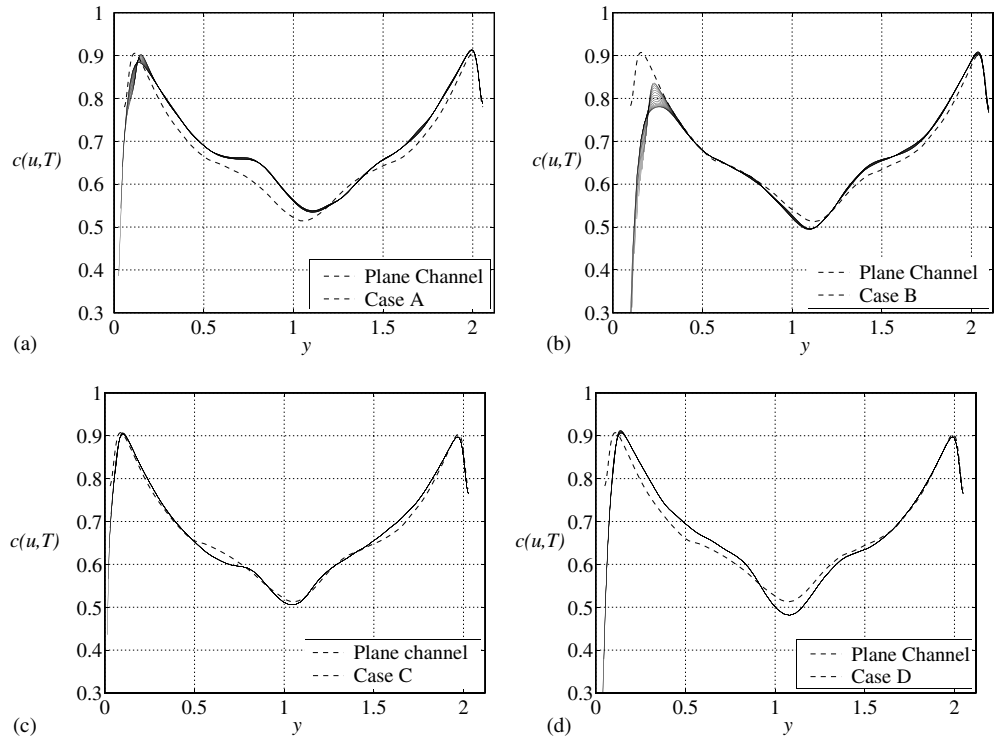

Fig. 17. Correlation coefficient between streamwise velocity and temperature for the four cases: (a) case A; (b) case B (c) case C; (d) case D. The comparison with the flat channel results is shown.

fluctuations in Figs. 5 and 6 are damped, or at least uninfluenced, by the presence of the drag-reducing riblets; this indicates that the turbulent activity is reduced, and the turbulent vertical heat flux term is not likely to contribute significantly to heat transfer, in particular in the drag-decreasing cases.

The total advective heat flux in vertical direction $\overline{v}\overline{T} + \overline{v'T'}$ is depicted in Figs. 11b, 11d, 12b and 12d. Isoflux lines are almost everywhere normal to the cross-flow mean velocity vectors; this is a clear indication that the convective heat flux follows the same paths of the secondary velocities.

5.3.7. Instantaneous drag and heat transfer patterns

Typical patterns of the instantaneous drag and temperature fluctuation on the riblet surfaces are illustrated, for $\alpha = 45°$, $s^+ = 20$ and $s^+ = 40$, in Fig. 15; the strong correlation of streamwise velocity and temperature gives raise to a marked similarity between the drag and temperature fluctuations. Drag increase areas, identified by bright spots, correspond to high heat transfer zones, and vice versa.

The instantaneous streamwise velocity and temperature fields in a cross-flow plane are dillustrated in Fig. 16 in case A and case C configurations. Again the two fields are well correlated; it can be noticed that, due to $Pr < 1$, the temperature field is slightly smoother than the streamwise velocity.

In order to investigate the relation between the streamwise velocity and the temperature fields over riblets, the correlation coefficient $c(u, T)$, defined as

$$c(u,T) = \frac{\overline{u'T'}}{\left(\overline{u'u'}\,\overline{T'T'}\right)^{1/2}} \tag{21}$$

is depicted in Fig. 17. It is not smaller over all riblet configurations than on the flat wall except for case B, where the low u–T correlation is associated with the lowest efficiency in drag and heat transfer. The minimum is reached in the valleys where the different boundary conditions have a stronger effect; the $c(u, T)$ correlation coefficient loses its meaning on the wall, where $u' = 0$.

6. Conclusions

The flow and heat transfer over riblets in both laminar and turbulent regimes is investigated by means of direct numerical simulation of the three dimensional, time dependent flow and energy equations. The simulations were performed over riblets of four different configurations, for a fluid with $Pr = 0.71$, representative of air.

The calculations in the laminar regime, where riblets are ineffective in reducing the skin friction, reveal that also the heat transfer effectiveness of the riblets is

slightly lower than that of a flat wall. In particular, the lowest efficiency is found on the riblets with the larger ridge angle. A highly accurate, two-dimensional FEM simulation is used to corroborate the laminar results and to preliminarily validate our DNS code.

The simulations in the turbulent regime are performed for a Reynolds number, based on the wall-shear velocity, $Re_\tau = 180$. The accuracy of the numerical procedure in turbulent flows is first checked by comparison of the computed results with some available correlations and past numerical works, for the case of flow and heat transfer in a plane channel.

In the simulation of the turbulent flow and heat transfer over riblets, all the mean flow features, the turbulent quantities, and the drag ratio D_r/D_f values, agree well with past experimental and numerical studies. The thermal field results, which do not follow some of the experimental findings (Walsh and Weinstein, 1979; Choi and Orchard, 1997), clearly show that the heat transfer efficiency of riblets, in the turbulent regime, is lower than that of a smooth wall at $Pr = 0.71$, thus further confirming the recent analysis of Benhalilou and Kasagi (1999). The reasons for the discrepancy with some of the experimental studies is unknown, but might indicate that the measurements were conducted in conditions far from complete thermal development, a basic assumption of our study.

The attainment of a favourable efficiency value $\eta > 1$ over riblets would be possible for high Prandtl fluids, where the thermal layer thickness becomes of the order of the riblets height. Further experimental and numerical investigations of heat transfer over riblets, for high Prandtl number fluids, should be carried out to clarify this aspect.

Acknowledgements

We wish to thank Prof. Nobuhide Kasagi of the Department of Mechanical Engineering, University of Tokyo, for having carefully read a preliminary version of the manuscript and for his enlightening comments. Financial support for this research was provided by ENEA—Contratto Settore Calcolo L.95/95—and is gratefully acknowledged. Part of the calculations have been performed on the SGI Origin 3800 at CINECA, Bologna.

References

Andersson, H., Kristoffersen, R., 1992. Statistics of numerically generated turbulence. Acta Appl. Math. 26, 293–314. Available from http://www.thtlab.t.u-tokyo.ac.jp/.

Baron, A., Quadrio, M., Vigevano, L., 1989. Riduzione della resistenza di attrito in correnti turbolente e altezza di protrusione di pareti scanalate. Aerotecnica missili e spazio, pp. 129–136.

Benhalilou, M., Kasagi, N., 1999. Numerical prediction of heat and momentum transfer over micro-grooved surface with a nonlinear k–ϵ model. Int. J. Heat Fluid Flow 42, 2525–2541.

Bhatti, M., Shah, R., 1987. Turbulent and transition flow convective heat transfer in ducts. In: Kakac, S., Shah, R., Aung, W. (Eds.), Handbook of Single-Phase Convective Heat Transfer. John Wiley & Sons, New York (Chapter 4).

Choi, K.-S., Orchard, D., 1997. Turbulence management using riblets for heat and momentum transfer. Exp. Thermal Fluid Sci. 15, 109–124.

Choi, H., Moin, P., Kim, J., 1991. On the effect of riblets in fully developed laminar channel flows. Phys. Fluids A 3, 1892–1896.

Choi, H., Moin, P., Kim, J., 1993. Direct numerical simulation of turbulent flow over riblets. J. Fluid. Mech. 225, 503–539.

Chu, D.C., Karniadakis, G.E., 1993. A direct numerical simulation of laminar and turbulent flow over riblet-mounted surfaces. J. Fluid. Mech. 250, 1–42.

Coustols, E., 1998. Main features of turbulent drag reduction via microgrooved surfaces: riblets. In: Papailiou, K., Tsahalis, D.K.D., Périaux, J. (Eds.), Computational Fluid Dynamics '98. John Wiley & Sons, Athens, Greece, pp. 594–603.

Femlab Reference Manual, 1999. http://www.femlab.com.

Ghia, K.N., Ghia, U., 1988. Elliptic systems: finite difference method iii. In: Minkowycz, W., Sparrow, E., Schneider, G., Pletcher, R. (Eds.), Handbook of Numerical Heat Transfer. John Wiley & Sons, New York (Chapter 8).

Goldstein, D., Tuan, T.-C., 1998. Secondary flow induced by riblets. J. Fluid. Mech. 363, 115–151.

Goldstein, D., Handler, R., Sirovich, L., 1995. Direct numerical simulation of turbulent flow over a modelled riblet covered surface. J. Fluid. Mech. 302, 333–376.

Gresho, P.M., 1990. On the theory of semi-implicit projection methods for viscous incompressible flow and its implementation via a finite element method that also introduces a nearly consistent mass matrix. Part 1. Theory. Int. J. Numer. Meth. Fluids 11, 587–620.

Jiménez, J., Moin, P., 1991. The minimal flow unit in near-wall turbulence. J. Fluid. Mech. 225, 213–240.

Kader, B., 1981. Temperature and concentration profiles in fully turbulent boundary layers. Int. J. Heat Mass Transfer 43, 1541–1544.

Kim, J., Moin, P., Moser, R., 1987. Turbulence statistics in fully developed channel flow at low Reynolds number. J. Fluid. Mech. 177, 133–166.

Launder, B., Li, S., 1993. On the prediction of riblet performance with engineering turbulence models. Appl. Sci. Res. 50, 283–298.

Lindemann, A., 1985. Turbulent Reynolds analogy factors for nonplanar surface microgeometries. J. Spacecraft 22, 581–582.

Maciejewski, P., Rivir, R., 1994. Effects of surface riblets and free-stream turbulence on heat transfer in a linear turbine cascade. ASME International Gas Turbine and Aeroengine Congress and Exposition, The Hague, Netherlands, pp. 1–9.

Nobile, E., Onesti, L., 1997. An efficient data parallel approach to finite volume simulation of buoyant flows. In: Liu, C., Liu, Z. (Eds.), Advances in DNS/LES. Ruston, Lousiana, USA, pp. 555–562.

Nobile, E., Stalio, E., Piller, M., 2000. Numerical simulation of heat transfer over riblets. In: Hahne, E., Heidemann, W., Spindler, K. (Eds.), Third European Thermal Sciences Conference, vol. 1, Heidelberg, Germany, pp. 313–318.

Piller, M., Nobile, E., 2002. Direct numerical simulation of turbulent heat transfer in a square duct. Int. J. Numer. Meth. Heat Fluid Flow 12 (6), 658–686.

Suzuki, Y., Kasagi, N., 1994. Turbulent drag reduction mechanism above a riblet surface. AIAA J. 32, 1781–1790.

Walsh, M., 1982. Turbulent boundary layer drag reduction using riblets. AIAA Paper (82-0169).

Walsh, M., Weinstein, L., 1979. Drag and heat transfer characteristics of small longitudinal ribbed surfaces. AIAA J. 17, 770–771.